CrossMark

INVITED ARTICLE

Spiky niobium oxide nanoparticles through hydrothermal synthesis

Teruaki Fuchigami[a)]
Department of Life Science and Applied Chemistry, Nagoya Institute of Technology, Nagoya 466-8555, Japan
Ken-ichi Kakimoto
Department of Life Science and Applied Chemistry, Nagoya Institute of Technology, Nagoya 466-8555, Japan; and Frontier Research Institute for Materials Science, Nagoya Institute of Technology, Nagoya 466-8555, Japan

(Received 1 January 2017; accepted 1 May 2017)

The development of ceramic nanomaterials with unique structure is necessary for discovery of novel property. We developed a novel niobium oxide nanoparticles with a spiky morphology. The spiky structure was composed of two kinds of component: niobium oxide hydrate sphere core and niobium pentoxide nanorods. These spiky niobium oxide nanoparticles are easily synthesized by hydrothermal treatment of niobium oxalate solution at 200 °C for 2 h, and their particle size could be tuned from 80 to 300 nm with 5–10 nm of nanorod on the surface by adjusting niobium concentration in the niobium oxalate solution. The band gap energy of the spiky nanoparticles was around 3.4 eV, and the spiky niobium oxide nanoparticles showed a light absorption in a wide wave length range from 380 to 700 nm. The niobium oxide nanoparticles are applicable as both solid acid catalyst and photocatalyst because of their spiky and two-layer structure.

I. INTRODUCTION

Ceramic nanomaterials with functional properties have attracted great interest in the development of sensors, catalyst, fuel cells, biomedicine, and data storage.[1–4] Over the past decades, various kinds of liquid-phase synthesis methods, such as sol–gel processes and hydrothermal methods, have been developed for synthesizing fine ceramic nanomaterials and controlling their size and crystal structures.[5–9] Recently, morphological control of functional nanomaterials have attracted much attention, and many ceramic nanomaterials with 0D (isotropic structure), 1D, 2D, or 3D (anisotropic structure) structures have been developed because there is a close relationship between the morphology and their properties.[10–13] For example, cobalt oxide with nano-rod structure showed higher oxidative catalytic activity than that of sphere-shaped cobalt oxide even under room temperature.[14] This is because atomic species or their combination affecting the catalytic activity was exposed on the particle surface by controlling the morphology. Thus, by controlling the nanostructure of existing materials, it is promising that development of novel functional materials and improvement of their properties. In addition, by using the ceramic nanomaterials as a precursor powder for thin film and bulk ceramics, not only the size but also the morphology of ceramic nanomaterial should affect the sintering behavior, and their final structures and properties should be changed. Therefore, development of novel shaped ceramic nanomaterials is important for all of the various fields.

Niobium oxide is widely used in biomedical, electric, and optical applications such as an implant material, a capacitor, and an interference filter because the niobium oxide has biocompatibility, corrosion resistance, high flame-retardant, wide-band-gap (E_g: 3.4 eV), high refraction factor and low reflectivity.[15–21] Niobium oxide powder, especially niobium pentoxide is also an important component of ferroelectric compounds such as $KNbO_3$, $NaNbO_3$, $LiNbO_3$, and (Na, K)NbO_3.[22–28] Furthermore, niobium oxide has a wide range of catalytic activities. Nakajima et al. reported $Nb_2O_5{\cdot}nH_2O$ functions as a heterogeneous catalyst with water-tolerant Lewis acid sites.[29] Photocatalytic activity of niobium oxide has been long studied, and it is reported that the photocatalytic activity depends on the morphology.[30,31] Therefore, various shaped niobium oxides, such as rod-, sheet-, and wire-shaped nanomaterials, have been synthesized through liquid-phase synthesis methods. Hydrothermal synthesis is one of the liquid-phase synthesis method and a powerful technique for the synthesis of both morphologically and crystallographically controlled ceramic oxide nanoparticles because a hydrolysis of starting materials and the crystallization of ceramic nanoparticles are accelerated by high temperature and high pressure conditions in an autoclave. In addition, organic surfactants are easily dissolved in the solvent and adsorbed on the surface of ceramic nanoparticles in the subcritical condition. Luo et al. synthesized single crystalline Nb_2O_5 nanorods by hydrothermal synthesis at 200 °C for 3–30 days using metal niobium powder and water. The nanorod are highly crystalline and they have well-controlled morphology (50 nm in

Contributing Editor: Nahum Travitzky
[a)]Address all correspondence to this author.
e-mail: fuchigami.teruaki@nitech.ac.jp
DOI: 10.1557/jmr.2017.200

https://doi.org/10.1557/jmr.2017.200 Published online by Cambridge University Press

 © Materials Research Society 2017

a diameter, several micrometers in length).[32] Fan et al. reported $N_2O_5{\cdot}nH_2O$ nanosheet synthesized through hydrothermal route. In this hydrothermal synthesis process, a presence of organic ammonium cations or NH^{4+} dissolved in subcritical water played an important role for the formation of sheet structure.[33]

We have synthesized "spiky" shaped niobium oxide nanoparticles by simple hydrothermal synthesis using niobium oxalate aqueous solution as the starting material. Spiky structure was composed of sphere core and numerous nanorod on the surface. Some of spiky-shaped ceramic nanomaterials have been reported but there are few reports for the unique structure.[34–36] Additionally, the study of the spiky-shaped niobium oxide is the first in the world as far as we searched. In this study, we have tried to control the size and morphology of the spiky-shaped niobium oxide nanoparticles by changing a niobium concentration in a starting solution, and discussed about the formation mechanism of spiky niobium oxide nanoparticles. The obtained powders were characterized by XRD and TEM to examine the unique two-layer structures. Thermal analysis and spectroscopic analysis were carried out for further structural characterization and investigation of optical property.

II. EXPERIMENTAL METHODS

A. Synthesis of spiky niobium oxide nanoparticles by hydrothermal methods

All chemicals are used without purification. Niobium oxalate aqueous solution was prepared as follows and used as a precursor solution.[37] Oxalic acid anhydrous (Kishida Chemicals, Osaka, Japan; 27.0 g) was dissolved in 300 mL of deionized water. Niobium(V) oxide hydrate (Mitsuwa's Pure Chemicals, Osaka, Japan; 2.7 g, Nb concentration: 17.0 mmol) was added into an oxalic acid solution (300 mL, 1.0 M). The solution was stirred at 105 °C for 5 h. Then, the niobium oxalate solution was diluted with deionized water to adjust the niobium concentration from 5 to 40 mM in the niobium oxalate solution. The diluted niobium oxalate solution was transferred into an autoclave (Mitsuai Chemistry, Sanai-Kagaku, Aichi, Japan; 25 mL in volume) to treat hydrothermally under autogeneous pressure. The autoclave was put in a mantle heater and heating it with stirring. Hydrothermal temperatures of 200 °C and heating duration of 2–20 h were used. After the treatment, the autoclave was removed from the mantle heater and cooled to room temperature. The products were recovered by centrifugation, washed with distilled water and finally dried at 60 °C for 12 h.

B. Powder characterization

The samples were characterized by the following techniques. Powder X-ray diffraction patterns (XRD) were recorded with a diffractometer (Philips X′per, PANalytical B.V., Almelo, the Netherlands) using Cu $K_{\alpha 1}$ radiation (voltage: 45 kV, current: 40 mA). The particle size and morphology of powders were determined by field Emission Scanning Electron Microscope (FE-SEM; JSM-7800F, JEOL Ltd., Tokyo, Japan) at 1 kV and transmission electron microscopy (TEM; JEM2100F, JEOL Ltd.) at 200 kV. Pt–Pd coating was carried out for FE-SEM observation. The thickness of Pt–Pd was adjusted to 0.5 nm. Infrared spectra of the nanoparticles were obtained using a Fourier transform infrared (FT-IR) analysis spectrometer (Jasco FT/IR-6300, JASCO Corporation, Tokyo, Japan) by KBr Pellet Method. Thermal analysis of the samples was carried out by simultaneous thermogravimetry/differential thermal analysis (TG-DTA) measurement (DTG-60H, SHIMADZU Corporation, Kyoto, Japan). The products before drying at 60 °C were dispersed in 50 mL of water, and optical absorption spectra of the product suspension were recorded with UV/VIS/NIR Spectrophotometer (UV-vis; V570, JASCO Corporation).

III. RESULTS AND DISCUSSION

XRD patterns of the obtained samples synthesized by hydrothermal treatment for 2 h from the niobium oxalate solution with different niobium concentration (5–40 mM) and niobium(V) oxide hydrate ($Nb_2O_5{\cdot}nH_2O$) purchased from Mitsuwa's Pure Chemicals were shown in Fig. 1. XRD pattern of the niobium oxide hydrate showed halo patterns around at $2\theta = 28.0$, 52.5, and 59.8°, confirming an amorphous feature of the conventional $Nb_2O_5{\cdot}nH_2O$. For the niobium oxide nanoparticles synthesized by hydrothermal treatment of niobium oxalate, tense and sharp peaks were observed at $2\theta = 22.6$ and 46.4° attributed to (001) and (002) planes of the pseudohexagonal structure (JCPDS card No. 28-0317), respectively, and broad peaks were also observed around at $2\theta = 25.9$ and 55.9°. These result indicates the niobium oxide nanoparticles synthesized from niobium oxalate in hydrothermal treatment were composed of crystalline niobium pentoxide grown in *c*-direction and the amorphous $Nb_2O_5{\cdot}nH_2O$. Figure 2 shows SEM images of niobium oxide nanoparticles synthesized by hydrothermal treatment for 2 h from niobium oxalate solution (Nb concentration: 40 mM). The niobium oxide nanoparticles had sphere-shaped core and numerous 1D nanorods grew radially on the surface of the sphere core particles (spiky shape). This result confirmed that the spiky shape was not formed by aggregation of the nanorods. Figure 3 show TEM images of the niobium oxide nanoparticles synthesized by changing niobium oxalate concentration. The reaction time was fixed for 2 h. Although, there was no significant difference between XRD patterns of the obtained niobium oxide particles, morphological nanostructures of the niobium oxide

https://doi.org/10.1557/jmr.2017.200 Published online by Cambridge University Press

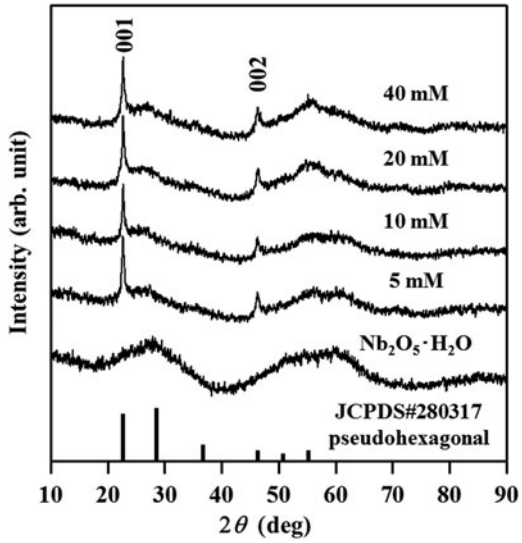


FIG. 1. XRD patterns of the niobium oxide nanoparticles synthesized in hydrothermal treatment of niobium oxalate solution for 2 h by changing niobium concentration in the solution from 5 to 40 mM.

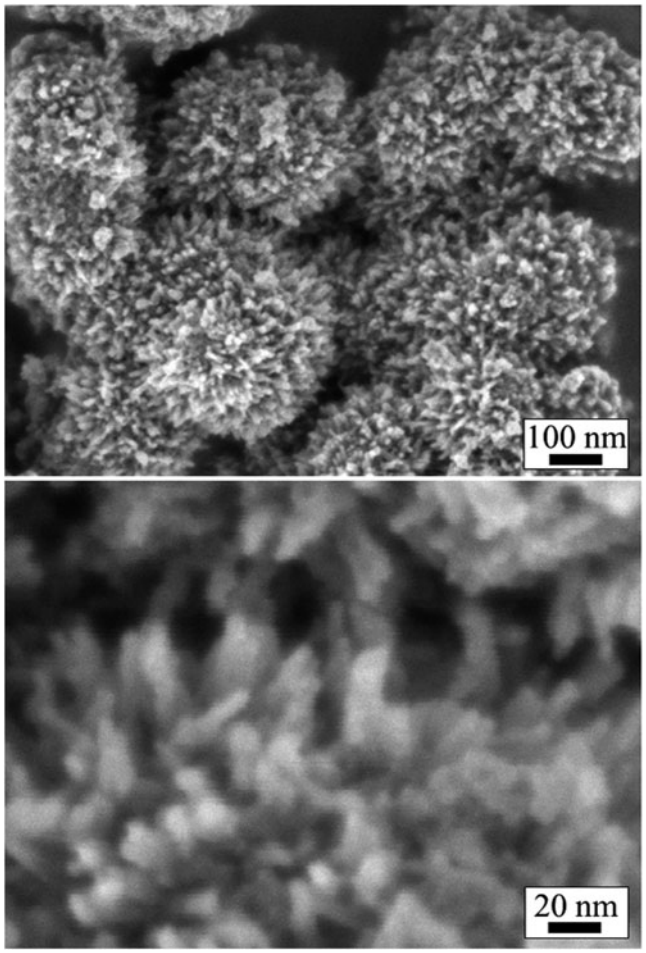


FIG. 2. SEM images of the spiky niobium oxide nanoparticles synthesized in hydrothermal treatment of niobium oxalate solution for 2 h (niobium concentration: 40 mM).

nanoparticles were completely different. Interestingly, although whole diameters of the spiky niobium oxide nanoparticles increased with increasing of niobium concentration, the diameters of nanorod were not changed. The average whole diameter (particle size) of the niobium oxide nanoparticles and the length of minor axis of the nanorods were calculated from 50 particles and summarized in Fig. 4. The average whole diameters of the niobium oxide nanoparticles synthesized from 5, 10, 20, 40 mM of niobium solution were 83, 148, 212, 297 nm, respectively. They were clearly increased by increasing niobium concentration. On the other hands, the average length of minor axis of the nanorods was around 5–10 nm, and it was relatively constant. Accordingly, the initial concentration of niobium oxalate affects only the core particle size, the nanorods are grown after the formation of the spherical core. We believed that the nanorods were grown in a dissolution-precipitation process of spherical core and the spiky niobium oxide nanoparticles were synthesized by changing the reaction time from 2 to 20 h. Figure 5 show the spiky niobium oxide nanoparticles synthesized by hydrothermal treatment for 2 and 20 h (Nb concentration: 6 mM) and had 155 ± 13.0 nm and 104 ± 9.4 nm in diameter, respectively. The particle sizes decreased with increasing reaction time from 2 to 20 h. The average lengths of minor axis of the nanorods on spiky nanoparticles treated for 2 h and 20 h were 5.3 ± 0.4 nm and 6.4 ± 1.2 nm, respectively. There was no significant difference between the average lengths of minor axis of the nanorods; however, tabular shaped nanocrystal was observed on the tip of nanorod for 20 h [Fig. 5(b)]. The tabular shaped nanocrystal was not adsorbed on the nanorod, but it was completely fused with the nanorod [Fig. 5(c)]. This result suggested that the tabular shaped nanocrystals were grown on the tip of nanorods. Given that the decrease of particle size and the morphology change with increasing reaction time, the niobium oxide nanoparticles were dissolved and re-crystallized during hydrothermal treatment. Additionally, the formation of tabular shaped nanocrystals suggested that the oxalic acid facilitates the formation of nanorods during extended period of reaction time. To reveal the presence and role of surfactant (oxalic acid ion) on the spiky niobium oxide nanoparticles, TG-DTA and infrared analyses were carried out on the samples. Figure 6 show TG-DTA curves and FT-IR spectrum of the spiky niobium oxide nanoparticles synthesized from niobium oxalate solution (Nb concentration: 20 mM). The first mass loss step occurs from 25 to 150 °C, also presenting an endothermal DTA peak [Fig. 6(a)]. This is attributed dissociation of combined water. 4% of weight loss in the first mass loss step also indicated the spiky niobium oxide nanoparticles were composed of $Nb_2O_5 \cdot nH_2O$ and niobium pentoxide. The second mass loss step occurs from 200 to 240 °C, also presenting an endothermal DTA peak. The third mass loss

https://doi.org/10.1557/jmr.2017.200 Published online by Cambridge University Press

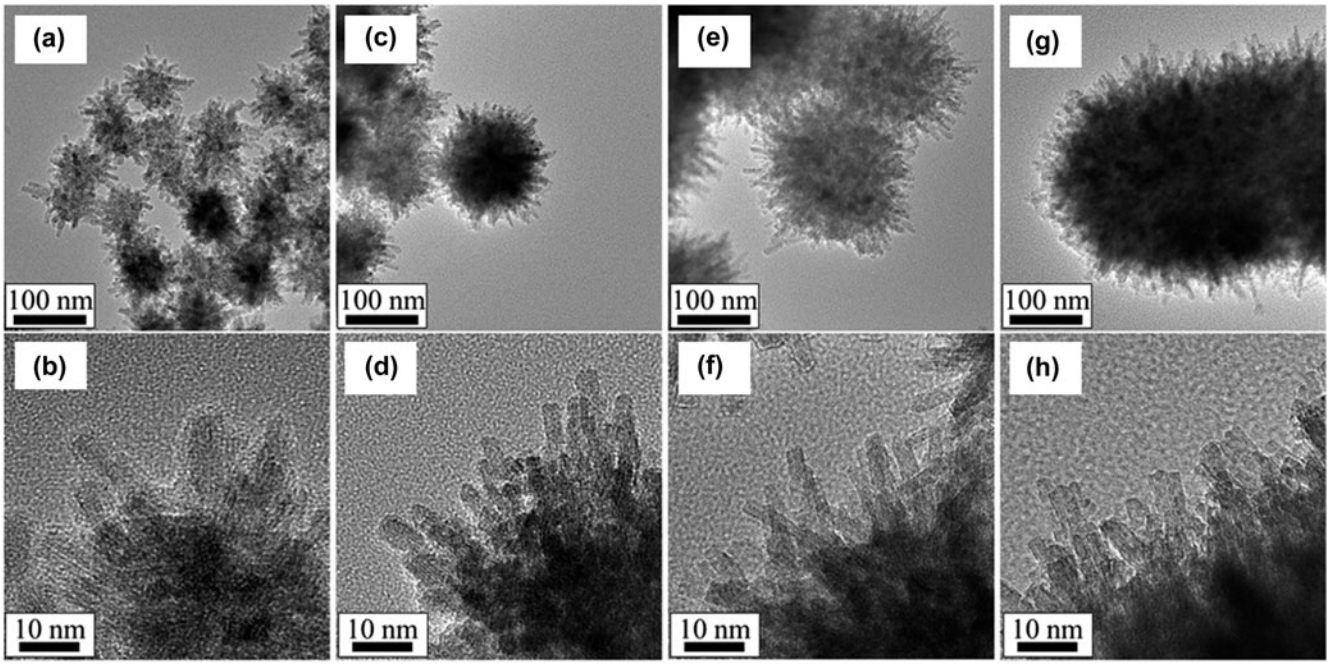


FIG. 3. TEM images of the spiky niobium oxide nanoparticles synthesized in hydrothermal treatment of niobium oxalate solution with different niobium concentration: (a, b) 5, (c, d) 10, (e, f) 20, and (g, h) 40 mM.

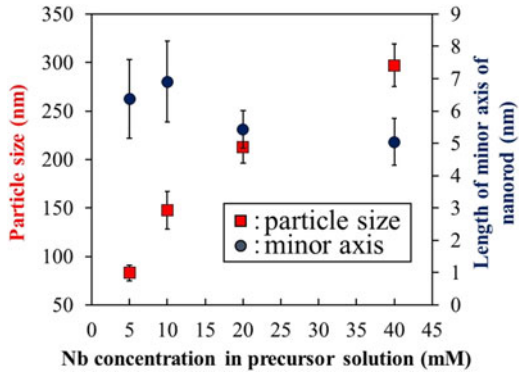


FIG. 4. Niobium concentration dependency of the particle size and the length of minor axis of the nanorods determined by TEM images of the spiky niobium oxide nanopaticles.

step occurs from 330 to 360 °C, presenting an exothermal DTA peak. Oxalic acid is decomposed into formic acid, carbon monoxide, and carbon dioxide at around 200 °C, and it is burned completely at around 300 °C. Therefore, oxalic acid was certainly adsorbed on the spiky nanoparticles. FT-IR analysis result also showed the existence of oxalic acid and combined H_2O as shown in Fig. 6(b). FT-IR spectrum of the spiky nanoparticles synthesized from niobium oxalate solution (Nb concentration: 20 mM) exhibit broad bands at around 1620 cm^{-1}, which can be attributed to a hydroxyl group of combined H_2O in/on the niobium oxide particles. Small peak at 1713 cm^{-1} in the FT-IR spectrum of the sample belonged to the C=O stretching mode of the carboxyl group. These results clearly shows oxalic acid played an important role in the formation of the spiky structure, and niobium oxide hydrate was included in the spiky nanoparticles.

From the results, we hypothesize that a formation mechanism of the spiky niobium oxide nanoparticles as follows. Figure 7 shows schematic illustration of formation mechanism of the spiky niobium oxide nanoparticles at low/high niobium concentration. First, $Nb_2O_5{\cdot}nH_2O$ are formed by hydrolysis of the niobium oxalate, and $Nb_2O_5{\cdot}nH_2O$ particles are agglomerated in a solution. Increasing the niobium concentration, a number of nuclei increases, consequently, the size of $Nb_2O_5{\cdot}nH_2O$ primary particles formed by agglomeration increase. The rod-shaped niobium pentoxide are grown on the surface of the sphere-shaped $Nb_2O_5{\cdot}nH_2O$ core particles. $Nb_2O_5{\cdot}nH_2O$ particles dissolve and precipitate again and again during the long hydrothermal treatment. In the dissolution-precipitation process, free-oxalic acid ions would be attached on *a–b* plane of niobium pentoxide, consequently, crystalline rod-shaped niobium pentoxide is grown on the surface. It is reported that rod-shaped niobium oxide obtained from ammonium niobium oxalate solution by hydrothermal treatment have a layered structure in the *c*-direction, and the oxalic acid contributes to the formation of rod-shaped particles.[38,39] The diameter of the nanorod doesn't change because all monomer ions (niobium oxalate ion) should be used for the formation of $Nb_2O_5{\cdot}nH_2O$ particles before the growing of the rod-shaped niobium pentoxide. Thus, if it is possible to control agglomeration, dissolution-precipitation, and

https://doi.org/10.1557/jmr.2017.200 Published online by Cambridge University Press

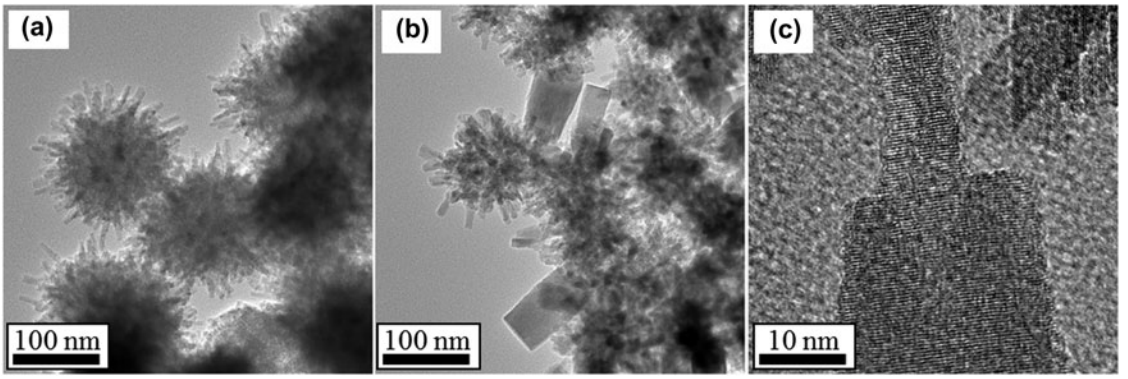


FIG. 5. TEM images of the spiky niobium oxide nanoparticles synthesized in hydrothermal treatment of niobium oxalate solution (niobium concentration: 6 mM) with different reaction time (a) 2 h, and (b, c) 20 h.

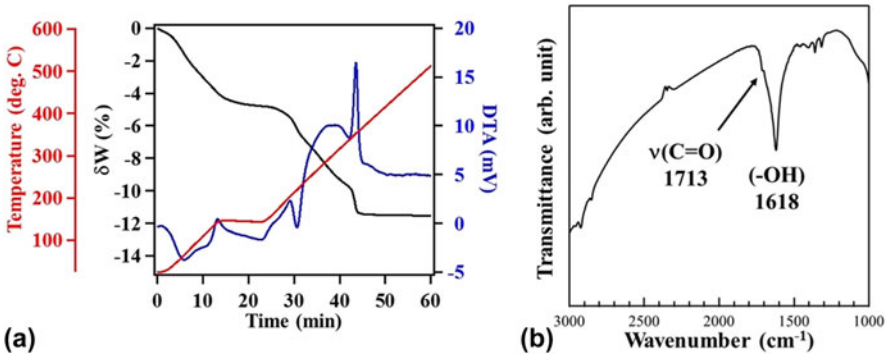


FIG. 6. (a) TG-DTA curve and (b) FT-IR spectra of the spiky niobium oxide nanoparticles synthesized in hydrothermal treatment of niobium oxalate solution for 2 h (niobium concentration: 20 mM).

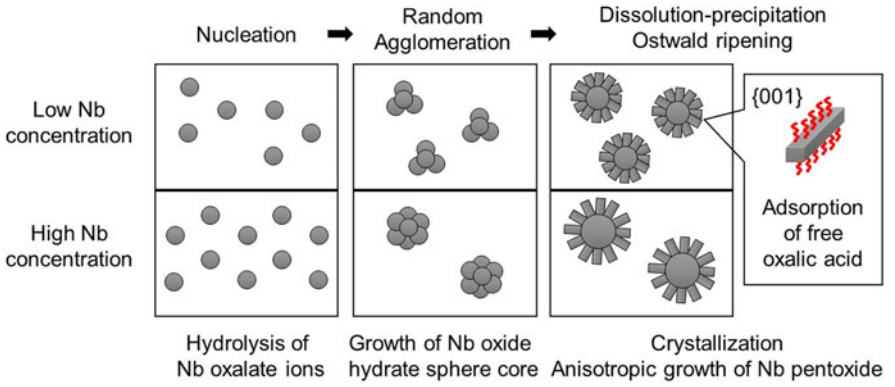


FIG. 7. Schematic illustration of step wise growth mechanism of spiky-shaped niobium oxide nanoparticles composed of sphere niobium oxide hydrate and rod-shaped niobium pentoxide.

particle growth process and to select a surfactant adsorb to specific plane, spiky shaped particles of any ceramics should be obtained.

Optical property of the spiky niobium oxide nanoparticles were investigated by UV-vis spectroscopy. Figure 8 shows UV-vis absorption spectra of the spiky niobium oxide nanoparticles with different particle sizes synthesized by changing Nb concentration from 5 to 40 mM. The spiky nanoparticles with 297 nm in average size showed broad absorption peak from 250 to 380 nm. The absorption peaks became sharp with decreasing particle size as shown Fig. 3, and peak wavelengths were slightly moved to at longer wave length. Furthermore, when the particles size decreased to less than 200 nm, wide range absorption was observed from 380 to 700 nm. Band gap energy calculated from their UV-vis absorption

https://doi.org/10.1557/jmr.2017.200 Published online by Cambridge University Press

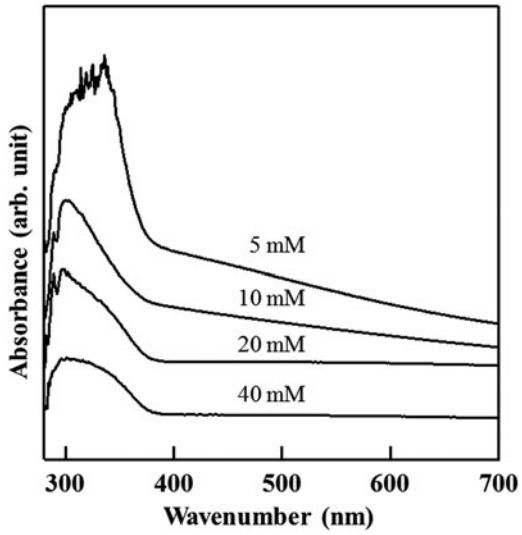


FIG. 8. UV-vis spectra of the spiky niobium oxide nanoparticles synthesized in hydrothermal treatment of niobium oxalate with different niobium concentration (5–10 mM).

TABLE I. Niobium concentration dependency of band gap energy and peak wave length.

Nb conc. (mM)	E_g (eV)	Peak wavelength (nm)
5	3.37	336
10	3.42	301
20	3.37	299
40	3.38	296

spectra and their peak wavelengths were summarized in Table I. Although decreasing particle size led to red shift of the absorption peak and to change the adsorption wave length region, band gap energies of the spiky nanoparticles with different particle sizes were almost same (3.37–3.42 eV). This is because the band gap depend on the size of the nanorod on the surface of spiky niobium oxide nanoparticles, and there was no significant difference between the diameters of the rod-shaped niobium pentoxide. These results also showed the spiky niobium oxide nanoparticles were assembled from two different component (the sphere core of niobium oxide hydrate and nanorod of niobium pentoxide), and the spiky nanoparticles have two different properties. In other words, our spiky shaped niobium oxide nanoparticle has two-layer structure, and it will show multifunctional properties. For instance, niobium oxide hydrate core would show solid acid activity, and niobium pentoxide nanorod would show photocatalytic property. Thus, the spiky oxide nanoparticles can be applied to a wide range of fields. Furthermore, the spiky niobium oxide nanoparticles should show higher photocatalytic activity. Zhao et al. reported crystalline TT phase N_2O_5 (pseudo-hexagonal) nanorod surface of higher surface acidity showed higher photocatalytic activity than that of nanospheres for methylene blue decomposition in aqueous solution.[40] Higher catalytic activities are expected because our spiky nanoparticles are composed of numerous pseudohexagonal niobium pentoxide nanorod and the unique structure will give large surface area.

IV. CONCLUSIONS

In this work, spiky-shaped niobium oxide particles were synthesized by hydrothermal treatment of niobium oxalate solution. Particle sizes of the spiky nanoparticles could be tuned from 300 to 80 nm in diameter with maintaining the nanorod structure (5–10 nm in length of minor axis) on the surface by changing niobium concentration in the niobium oxalate solution. Thermal analysis and FT-IR analysis indicated the spiky niobium oxide nanoparticles were composed of sphere core particle of niobium oxide hydrate and niobium pentoxide nanorod, and free oxalic acid ions in the starting solution affected the formation of rod structure. The spiky niobium oxide nanoparticles showed the broad absorption peak from 250 to 400 nm, and red shift of the absorption peak and change of the adsorption wave length region were observed by decreasing particle size. Bang gap energies of the spiky nanoparticles were 3.37–3.42 eV, and they were not changed by decreasing particle size. We concluded the spiky niobium oxide nanoparticles are composed of two different ingredients, and the unique crystallographic and morphological structures are advantageous for a variety of different applications especially as catalyst.

REFERENCES

1. B. Kumara and S.W. Kim: Energy harvesting based on semiconducting piezoelectric ZnO nanostructures. *Nano Energy* **1**, 342–355 (2012).
2. K. Mimura and K. Kato: Enhanced dielectric properties of $BaTiO_3$ nanocube assembled film in metal–insulator–metal capacitor structure. *Appl. Phys. Express* **7**, 061501 (2014).
3. K.M.L. Taylor-Pashow, J.D. Rocca, R.C. Huxford, and W. Lin: Hybrid nanomaterials for biomedical applications. *Chem. Commun.* **46**, 5832–5849 (2010).
4. J. Lv, T. Kako, Z. Li, Z. Zou, and J. Ye: Synthesis and photocatalytic activities of $NaNbO_3$ rods modified by In_2O_3 nanoparticles. *J. Phys. Chem. C* **114**, 6157–6162 (2010).
5. S. Uchida, Y. Inoue, Y. Fujishiro, and T. Sato: Hydrothermal synthesis of $K_4Nb_6O_{17}$. *J. Mater. Sci.* **33**, 5125 (1998).
6. C.H. Lu, S.Y. Lo, and H.C. Lin: Hydrothermal synthesis of nonlinear optical potassium niobate ceramic powder. *Mater. Lett.* **34**, 172–176 (1998).
7. J.F. Liu, X.L. Li, and Y.D. Li: Novel synthesis of polymorphous nanocrystalline $KNbO_3$ by a low temperature solution method. *J. Nanosci. Nanotechnol.* **2**, 617 (2002).
8. S. Lee, T. Park, G. Choi, K. Koo, and W. Kim: Effects of KOH/BaTi and Ba/Ti ratios on synthesis of $BaTiO_3$ powder by coprecipitation/hydrothermal reaction. *Mater. Chem. Phys.* **82**, 742 (2003).
9. A. Sehgal, Y. Lalatonne, J-F. Berret, and M. Morvan: Precipitation-redispersion of cerium oxide nanoparticles with poly(acrylic acid): Toward stable dispersions. *Langmuir* **21**, 9359–9364 (2005).

https://doi.org/10.1557/jmr.2017.200 Published online by Cambridge University Press

10. C. Burda, X.B. Chen, R. Narayaman, and M.A. El-Sayed: Chemistry and properties of nanocrystals of different shapes. *Chem. Rev.* **105**, 1025–1102 (2005).
11. L. Zhang and Y.J. Zhu: Microwave-assisted solvothermal synthesis of AlOOH hierarchically nanostructured microspheres and their transformation to γ-Al_2O_3 with similar morphologies. *J. Phys. Chem. C* **112**, 16764 (2008).
12. Z.L. Wang and J.H. Song: Piezoelectric nanogenerators based on zinc oxide nanowire arrays. *Science* **312**, 242 (2006).
13. V. Polshettiwar, B. Baruwati, and R.S. Varma: Self-assembly of metal oxides into three-dimensional nanostructures: Synthesis and application in catalysis. *ACS Nano* **3**(3), 728–736 (2009).
14. X. Xie, Y. Li, Z-Q. Liu, M. Haruta, and W. Shen: Low-temperature oxidation of CO catalysed by Co_3O_4 nanorods. *Nature* **458**, 746–749 (2011).
15. Y.D. Wang, L.F. Yang, Z.L. Zhou, Y.F. Li, and X.H. Wu: Effects of calcination temperature on latice constants and gas sensing properties of Nb_2O_5. *Mater. Lett.* **49**, 277 (2001).
16. P. Carniti, A. Gervasini, and M. Marzo: Dispersed NbO_x catalytic phases in silica matrixes: Influence of niobium concentration and preparative route. *J. Phys. Chem. C* **112**, 14064 (2008).
17. S.H. Mujawar, A.I. Inamdar, S.B. Patil, and P.S. Patil: Electrochromic properties of spray-deposited niobium oxide thin films. *Solid State Ionics* **177**, 3333 (2006).
18. R. Jose, V. Thavasi, and S. Ramakrishna: Metal oxides for dyesensitized solar cells. *J. Am. Ceram. Soc.* **92**, 289 (2009).
19. K.S. Ahn, M.S. Kang, J.K. Lee, B.C. Shin, and J.W. Lee: Enhanced electron diffusion length of mesoporous TiO_2 film by using Nb_2O_5 energy barrier for dye-sensitized solar cells. *Appl. Phys. Lett.* **89**, 013103 (2006).
20. A.C. Mackey, R.L. Karlinsey, T.G. Chu, M. MacPherson, and D.L. Alge: Development of niobium oxide coatings on sand-blasted titanium alloy dental implants. *Mater. Sci. Appl.* **3**, 301–305 (2012).
21. A. Llordés, G. Garcia, J. Gazquez, and D.J. Milliron: Tunable near-infrared and visible-light transmittance in nanocrystal-in-glass composites. *Nature* **500**, 323–326 (2013).
22. Y. Guo, K. Kakimoto, and H. Ohsato: Phase transitional behavior and piezoelectric properties of $(Na_{0.5}K_{0.5})NbO_3$–$LiNbO_3$($Na_{0.5}K_{0.5}$)NbO_3–$LiNbO_3$ ceramics. *Appl. Phys. Lett.* **85**, 4121 (2004).
23. Y. Saito, H. Takao, T. Tani, T. Nonoyama, K. Takatori, T. Homma, T. Nagaya, and M. Nakamura: Lead-free piezoceramics. *Nature* **432**, 84–87 (2004).
24. T.R. Shrout and S.J. Zhang: Lead-free piezoelectric ceramics: Alternatives for PZT? *J. Electroceram.* **19**, 113–126 (2007).
25. G. Vats and R. Vaish: Selection of optimal sintering temperature of $K_{0.5}Na_{0.5}NbO_3$ ceramics for electromechanical applications. *J. Asian Ceram. Soc.* **2**, 5–10 (2014).
26. D. Mohanty, G. Chaubey, A. Yourdkhani, S. Adireddy, G. Caruntu, and J. Wiley: Synthesis and piezoelectric response of cubic and spherical $LiNbO_3$ nanocrystals. *RSC Adv.* **2**, 1913–1916 (2012).
27. K. Saito and A. Kudo: Niobium-complex-based syntheses of sodium niobate nanowires possessing superior photocatalytic properties. *Inorg. Chem.* **49**, 2017–2019 (2010).
28. H. Zhu, Z. Zheng, X. Gao, Y. Huang, Z. Yan, J. Zou, H. Yin, Q. Zou, S.H. Kable, J. Zhao, Y. Xi, W.N. Martens, and R.L. Frost: Structural evolution in a hydrothermal reaction between Nb_2O_5 and NaOH solution: From Nb_2O_5 grains to microporous $Na_2Nb_2O_6/3H_2O$ fibers and $NaNbO_3$ cubes. *J. Am. Chem. Soc.* **128**, 2373–2384 (2006).
29. K. Nakajima, Y. Baba, R. Noma, M. Kitano, J.N. Kondo, S. Hayashi, and M. Hara: Nb_2O_5 nH_2O as a heterogeneous catalyst with water-tolerant Lewis acid sites. *J. Am. Chem. Soc.* **133**, 4224–4227 (2011).
30. A.G.S. Prado, L.B. Bolzon, C.P. Pedroso, A.O. Moura, and L.L. Costa: Nb_2O_5 as efficient and recyclable photocatalyst for indigo carmine degradation. *Appl. Catal., B* **82**, 219–224 (2008).
31. J. Wu, J. Li, X. Lü, L. Zhang, J. Yao, F. Zhang, F. Huang, and F. Xu: A one-pot method to grow pyrochlore $H_4Nb_2O_7$-octahedron-based photocatalyst. *J. Mater. Chem.* **20**, 1942–1946 (2010).
32. H. Luo, M. Wei, and K. Wei: Synthesis of Nb_2O_5 nanorods by a soft chemical process. *J. Nanomater.* **2009**, 1–4 (2009).
33. W. Fan, Q. Zhang, W. Deng, and Y. Wang: Niobic acid nanosheets synthesized by a simple hydrothermal method as efficient brønsted acid catalysts. *Chem. Mater.* **25**, 3277–3287 (2013).
34. M.Y. Rafique, L. Pan, W.S. Khan, M.Z. Iqbal, H. Qiu, M.H. Farooq, M. Ellahi, and Z. Guo: Controlled synthesis, phase formation, growth mechanism, and magnetic properties of 3-D CoNi alloy microstructures composed of nanorods. *CrystEngComm* **15**, 5314–5325 (2013).
35. J. Yin, X. Zhao, L. Xiang, X. Xia, and Z. Zhang: Enhanced electrorheology of suspensions containing sea-urchin-like hierarchical Cr-doped titania particles. *Soft Matter* **5**, 4687–4697 (2009).
36. Y. Ye, J. Chen, Q. Ding, D. Lin, R. Dong, L. Yang, and J. Liu: Sea-urchin-like Fe_3O_4@C@Ag particles: An efficient SERS substrate for detection of organic pollutants. *Nanoscale* **5**, 5887–5895 (2013).
37. E.R. Camargo and M. Kakihana: Low temperature synthesis of lithium niobate powders based on water-soluble niobium malato complexes. *Solid State Ionics* **151**, 413–418 (2002).
38. T. Murayama, J. Chen, J. Hirata, K. Matsumoto, and W. Ueda: Hydrothermal synthesis of octahedra-based layered niobium oxide and its catalytic activity as a solid acid. *Catal. Sci. Technol.* **4**, 4250–4257 (2014).
39. T. Fuchigami and K. Kakimoto: Synthesis of niobium pentoxide nanoparticles in single flow supercritical water. *Jpn. J. Appl. Phys.* **55**, 10TB06 (2016).
40. Y. Zhao, C. Eley, J. Hu, J.S. Foord, L. Ye, and H. He: Shape-dependent acidity and photocatalytic activity of Nb_2O_5 nanocrystals with active TT (001) surface. *Angew. Chem., Int. Ed.* **51**, 3846–3849 (2012).

https://doi.org/10.1557/jmr.2017.200 Published online by Cambridge University Press